ATMOSPHERIC ENVIRONMENT: X 30 (2026) 100431

Contents lists available at ScienceDirect

Atmospheric Environment: X

journal homepage: www.journals.elsevier.com/atmospheric-environment-x

Chemical and size-resolved signatures of firework smoke in an urban atmosphere

Francesca Picca *, Fabio Sasso, Andrea D'Anna

Dipartimento di Ingegneria Chimica, dei Materiali e della Produzione Industriale, Università degli Studi di Napoli Federico II, Napoli, 80125, Italy

ARTICLE INFO

Keywords:
Urban air quality
Episodic emissions
Pyrotechnics
Sports victory celebration
Exposure assessment
HR-ToF-AMS
Optical particle sizer

ABSTRACT

Aerosol particles significantly influence atmospheric composition and urban air quality, yet episodic and non-conventional anthropogenic sources, such as pyrotechnics, remain less well characterized. These events can emit gaseous pollutants and fine particulate matter containing metals and organic additives, posing acute exposure risks in densely populated areas. This study presents an observational characterization of the atmospheric impact associated with the celebrations following the Italian football championship in Naples on May 23, 2025, providing a real-world case study of large-scale pyrotechnic and smoke-bomb use in an urban environment. Continuous monitoring from 22 to May 31, 2025 employed a High-Resolution Time-of-Flight Aerosol Mass Spectrometer with a Soot-Particle module and an Optical Particle Sizer. During the peak celebration night, major aerosol constituents increased rapidly. Chemical analysis revealed distinct pyrotechnic signatures, including pronounced chlorine enrichment, concurrent spikes in coloured-formulation metal tracers (Ba, Sr, Cu), enhanced hydrocarbon fragments, and smoke-bomb combustion markers. Elemental analysis indicated a shift toward less-oxidized organic aerosol, consistent with fresh primary-combustion input. Size-resolved data showed that PM mass increased primarily in the accumulation mode. In contrast, particle number increased most strongly in the submicron fraction, implying a dual exposure concern: elevated mass burden and fine-particle concentrations. Although total PM mass decayed rapidly, aerosol chemical composition remained perturbed. These findings demonstrate that large-scale pyrotechnic use creates acute, chemically complex pollution episodes with significant implications for urban air quality. Compared with another major fireworks event, New Year's Eve 2025 in Naples, the celebration exhibited a lower peak in PM2.5 but more persistent compositional anomalies, underscoring the need for integrated chemical- and size-resolved monitoring to assess episodic urban emissions beyond standard regulatory metrics. Unlike typical single-night fireworks, this multi-night, city-wide celebration represents a non-conventional pyrotechnic episode, in which mass concentrations recover quickly while aerosol composition and size properties remain perturbed for several days.

1. Introduction

The chemical and physical characteristics of aerosol particles significantly influence local air quality and public health. (Pöschl, 2005; Pope, 2006; Intergovernmental Panel on Climate Change (IPCC), 2023; Charlson et al., 1992; Lionetto et al., 2021). While extensive research has provided substantial insights into aerosols from common sources, knowledge regarding particles from less conventional anthropogenic sources remains limited in scientific literature (Zhang et al., 2011).

Fine particles can originate directly from primary emissions, such as fossil fuel combustion and biomass burning, or indirectly from the atmospheric oxidation of gas-phase species (Seinfeld and Pandis, 2016). Fireworks and pyrotechnic devices represent significant primary sources that can exert substantial short-term impacts on air quality. Indeed, fireworks are known to cause sharp, short-term increases in ambient particulate matter (PM) and associated aerosol chemical tracers (Zhang et al., 2019). Their combustion releases a large quantity of gaseous pollutants, including sulphur dioxide (SO_2) and nitrogen oxides (NOx) (Vecchi et al., 2008; Jiang et al., 2015; Huang et al., 2012). They emit fine particulate matter composed of organic/elemental carbon, sulphates, potassium, chlorides, and various metals such as copper (Cu), barium (Ba), strontium (Sr), and magnesium (Mg) (Moreno et al., 2007; Wang et al., 2007a; Liu et al., 1997; Perry, 1999; Kulshrestha et al., 2004). This enhanced short-term air pollution, often visible as dense

* Corresponding author.
E-mail address: francesca.picca@unina.it (F. Picca).

https://doi.org/10.1016/j.aeaoa.2026.100431
Received 8 January 2026; Received in revised form 13 February 2026; Accepted 26 February 2026
Available online 3 March 2026

smoke clouds, can reduce visibility for several hours. Beyond atmospheric concerns, the deposition of heavy metals from fireworks can also contaminate surface water, potentially causing extensive damage to vegetation and posing risks to human health, particularly in terms of short-term exposure during peak concentrations (Vecchi et al., 2008; Moore et al., 2014).

In the present study, however, such pyrotechnic episodes are regarded as acute, short-term perturbations superimposed on the broader urban pollution background. Their main relevance lies in elucidating source signatures, atmospheric processing and transient exposure peaks, rather than in representing a chronic air-quality or long-term health driver on their own.

Previous studies of fireworks have focused on specific festivals (e.g., Chinese Spring Festival, U.S. Independence Day, New Year's fireworks) (Zhang et al., 2019; Jiang et al., 2015; Retama et al., 2019; Drewnick et al., 2006a). These works consistently report intense spikes in K+, Cl–, metal tracers, and organic and inorganic aerosol mass during fireworks, often with rapid post-event oxidation (e.g., rising nitrate and sulphate the following day). A common observation is that firework organics usually exhibit a highly oxidized spectrum resembling secondary organic aerosol (SOA) (Zhang et al., 2019) and that photochemical reactions convert accumulated radicals into new nitrate, sulphate, and organics by morning (Retama et al., 2019).

Given these environmental and health concerns, the pollution resulting from pyrotechnic devices has recently garnered considerable attention within the scientific community. Previous studies have reviewed the effects of fireworks on air quality during specific festivals, summarizing pollution characteristics in terms of chemical components and health impacts (Zhang et al., 2019; Jiang et al., 2015; Faber et al., 2013). Other research has highlighted fireworks as a major contributor to environmental perchlorate contamination (Cao et al., 2018). However, there remains a knowledge gap concerning the specific pollution characteristics of various chemical components and emissions from pyrotechnic events, particularly in unique social contexts.

The study aims to assess the environmental impact of a significant social event, the celebration of the Naples football team's Scudetto victory on the evening of May 23, 2025, on local air quality. The event was characterized by the intense and widespread use of smoke bombs and fireworks, providing a unique opportunity to investigate the localized, short-term atmospheric effects of such activities in a densely populated urban environment. By focusing on this specific episode, we aim to enhance the understanding of pollution patterns and to evaluate their potential implications for environmental quality.

While numerous studies have documented the short-term impact of fireworks on urban air quality during highly localized and temporally confined events (e.g., New Year's Eve or national festivals), far less attention has been devoted to prolonged, spatially distributed pyrotechnic episodes occurring outside these traditional contexts. The celebrations following the SSC Napoli championship victory represent a markedly different emission scenario, characterized by multi-day duration, widespread deployment of fireworks, flares, and smoke bombs across the metropolitan area, and sustained human activity, rather than a single, centralized display.

This unique setup allows investigation of aspects typically inaccessible in traditional fireworks research. These include the disconnect between PM mass levels and chemically resolved aerosol recovery, the lasting effects of compositional changes even after PM2.5 levels approach pre-event values, and the simultaneous presence of mass-dominated and number-dominated exposure routes across various particle sizes. By integrating high-resolution chemical data from an HR-ToF-AMS (with SP-AMS features) and size-specific particle counts from an OPS, the study provides a comprehensive, real-world analysis of a sporadic yet prolonged urban pyrotechnic pollution event. This approach bridges the gap between brief fireworks displays and more widespread urban pollution conditions.

Here, we report simultaneous measurements of particle number concentrations (up to 10 μm) conducted using an Optical Particle Sizer (OPS), along with size-resolved chemical characterization of the refractory components of particulate matter (up to 2.5 μm) using a High-Resolution Time-of-Flight Aerosol Mass Spectrometer (HR-ToF-AMS). The co-deployment of these instruments in a real urban environment allows us to follow the evolution of both chemical composition and particle size. Measurements were performed at ground level in the city of Naples at our laboratory facility. Naples is a Mediterranean port city with complex emissions sources and sea-breeze influences. The dataset covers the period from the 22nd to the May 31, 2025, allowing observation of conditions before the event and of the evolution of atmospheric composition during and after the celebration. Particular attention is given to the identification of key particulate species associated with fireworks and smoke bomb emissions. These findings underscore how large-scale celebratory events can significantly alter the physicochemical properties of the atmosphere, with potential effects persisting for several days after the occurrence. In addition, we assess how this episode compares with typical PM2.5 variability in the city during a particular event, such as New Year's night (CS, 2025).

2. Experimental methods

2.1. Sampling site

Aerosol data were collected from the 22nd to the May 31, 2025. This measurement period encompassed SSC Napoli's “Scudetto” victory, the local Serie A soccer team, and the extensive fan celebrations that followed throughout the Naples metropolitan area. The measurements presented in this study were performed at the Centro Servizi Metrologici e Tecnologici Avanzati (CeSMA) of the Università di Napoli Federico II (40°50′14.6″N, 14°18′25.6″E). The sampling site is located at ground level in a densely populated neighborhood of the city, approximately 5 km from the city centre and 10 km from the stadium. During the celebration period, fireworks were widely discharged across the metropolitan area, both in the vicinity of the sampling site and at more distant locations.

While pyrotechnic emissions during the celebrations were spread across the Naples metropolitan area, measurements were taken at a single urban site. Therefore, these observations should be seen as representative of local exposure conditions in a densely populated inner-city neighborhood, rather than as a detailed spatial analysis of the entire metropolitan area. Because the sources are very diverse, the CeSMA site captures a specific part of the urban plume, offering detailed insights into the chemical changes of the aerosol at ground level. The meteorological conditions taken from the “Osservatorio Meteorologico San Marcellino” during the measurement period are reported in Fig. 1. Averaged wind speeds at the ground surface were generally below 15 km/h, with the highest value recorded during the night of celebrations. Ambient temperatures were consistent with the seasonal average, ranging between 20 $^{\circ}C$ and 25 $^{\circ}C$. These meteorological conditions are typical of late-spring anticyclonic stagnation, which is conducive to pollutant accumulation and limited dispersion. Similar meteorological scenarios have been documented in previous air quality assessments conducted during large-scale festive events, such as New Year's Eve celebrations (CS, 2025), when ARPAC reported the presence of a persistent high-pressure system and calm atmospheric conditions over Naples, resulting in particulate matter concentrations significantly exceeding regulatory thresholds (CS, 2025). Although the present observations were carried out in a different season, comparable stagnation processes are likely to have occurred. In particular, the limited nocturnal dispersion associated with calm conditions would have promoted the accumulation of firework-related emissions near ground level.

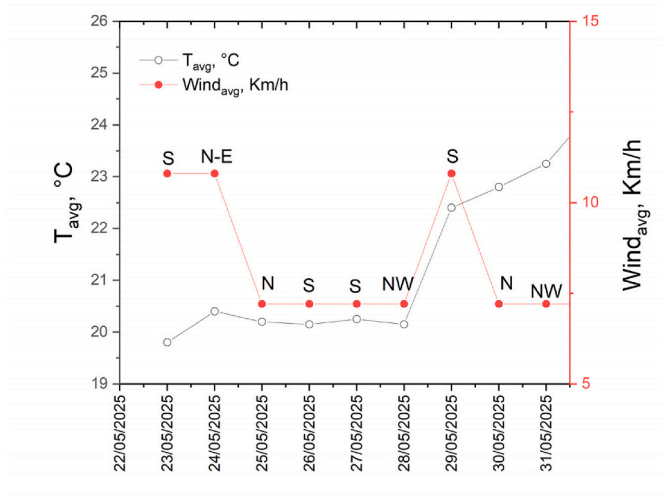

Fig. 1. Recorded meteorological conditions during the measurement period. Temperature is plotted on the left axis (grey line, °C); maximum wind speed is plotted on the right axis (red line, km/h). S, N, W, E stand for the four cardinal points. (For interpretation of the references to colour in this figure legend, the reader is referred to the Web version of this article.)

2.2. Experimental set-up

2.2.1. High resolution – time of flight – aerosol mass spectrometer

An HR-ToF-AMS (Aerodyne Research Inc.) is used to perform analyses of atmospheric aerosols. The instrumentation provides real-time data on the mass, chemical composition, and size of submicron atmospheric aerosol particles. A full description of the instrument is reported in (Jayne et al., 2000; DeCarlo et al., 2006a; Canagaratna et al., 2007).

Aerosol particles enter at a flow rate of 0.082 l min^{-1} through a 100 μm critical orifice, pass through the aerodynamic lenses (PM2.5 lenses), which focus them into a narrow beam. The PM2.5 aerodynamic lenses ensure ~100% transmission efficiency for particles between 100 and 2500 nm, with gradual roll-off beyond ~2.5 μm (Xu et al., 2017). Upon exiting the ToF section, particles are vaporized in a capture vaporizer heated to 600 °*C*. This ensures complete vaporization of non-refractory materials through multiple reflections within the cavity. The resulting vapor plume is then ionized by 70 eV electrons from a tungsten filament, generating singly positive charged ions. To achieve a comprehensive analysis of environmental composition, including refractory materials like metals and black carbon, an additional component is employed: the Soot Particle Aerosol Mass Spectrometer (SP-AMS) module. This module utilizes an intracavity Nd: YAG laser vaporizer (1064 nm) for high-irradiance vaporization (Baumgardner et al., 2004). The SP-AMS module selectively measures the mass of refractory black carbon cores and the mass and chemical composition of any coating materials (e.g., organics, sulphates, nitrates). This is achieved through laser-induced incandescence (LII) (Onasch et al., 2012). The intracavity laser, powered by an 808 nm free-beam pump laser, delivers a power density exceeding 0.2 MW/cm^2 (Drewnick et al., 2009; DeCarlo et al., 2006b). An acquisition time of 2 h was chosen to obtain aerosol properties representative of the urban air mass rather than highly localized and short-lived fireworks plumes. In densely populated urban environments, fireworks emissions are spatially heterogeneous and are transported intermittently beyond the sampling site. Longer averaging intervals reduce the influence of transient encounters with plumes and provide a more spatially and temporally integrated characterization of the aerosols experienced by the urban population.

Detection limits depend on the chemical species and integration time. For the HR-ToF-AMS in V-mode, the nominal 1-min detection limit for nitrate is approximately 0.003 μg m^{-3}, with higher limits for organics, sulphate, and ammonium (Drewnick et al., 2009; DeCarlo et al., 2006b). In this study, 2-h averaging yielded substantially lower effective detection limits than 1-min data. Consequently, trace-level species detected using the SP-AMS configuration (e.g., Ba^+, Sr^+, Cu^+) were close to the instrumental detection limit during background periods but clearly exceeded background noise during the celebration night. The HR-ToF-AMS was calibrated for inlet flow, ionization efficiency (IE), and particle sizing following the manufacturer's standard protocols (Jayne et al., 2000; Allan et al., 2003; Drewnick et al., 2005, 2015). Ammonium nitrate calibrations established ionization sensitivity and particle transmission.

2.2.2. Optical Particle Sizer

Particle number concentration and size distribution were measured using a TSI Model 3330 OPS, a lightweight, portable spectrometer that employs single-particle counting. The OPS samples at a flow rate of 1 L min^{-1}, measuring particles in the range of 0.3 μm to 10 μm across 16 user-adjustable size channels. The aerosol sample enters through an inlet nozzle at ambient relative humidity, as no upstream dryer was used, and is directly drawn into the measurement region to minimize transport losses. Inside the chamber, individual particles cross a laser beam, and the scattered light is collected by an elliptical mirror and detected by a photodetector. The intensity of the scattered pulse is used to determine particle number and optical-equivalent diameter according to Mie scattering theory. Consequently, particle size and derived mass can be affected by hygroscopic growth at elevated relative humidity and by particle morphology. For non-spherical fractal aggregates typical of pyrotechnic emissions, optical sizing may underestimate physical diameter, whereas water uptake may shift the optical diameter to larger values. To convert OPS number distributions into mass concentrations, an effective density (ρ_{eff}) of 1.4 g cm^{-3} was assumed. While this is a standard approximation for mixed urban aerosols, the presence of a specific chemical signature of pyrotechnic emissions, characterized by heavy metal salts and fractal soot aggregates, can introduce uncertainty in absolute mass quantification. The impact of this assumption on the robustness of our results, including sensitivity considerations, is further discussed in the Results section (Section 3.6).

2.3. Data analysis

Data processing was performed using SQUIRREL (version 1.55) and PIKA (version 1.14). Mass accuracy was calibrated using nitrogen atoms (m/z 14.003), nitrogen molecules (m/z 28.006), and tungsten (m/z 183.951). A collection efficiency of unity (CE = 1) was assumed for the capture vaporizer to estimate aerosol mass concentrations across all experiments accurately (Hu et al., 2018; Joo et al., 2021). The acquisition of data through the AMS enables evaluation of signals between 12 and 120 m/z with mass resolving power up to 2500 (high-resolution region). It is worth noting that the instrument detects only positively charged ion fragments produced by high-energy electron impact; thus, the species are identified in the mass spectra via their characteristic positive fragment ions and quantitatively inferred from known fragmentation patterns (Drewnick et al., 2005).

Aerosol-phase concentrations of key chemical components were estimated using an established reconstruction method that considers the relative ionization efficiency (RIE) of each species. Here, "species" refers to the chemically resolved parent neutral components, such as organic matter, sulphate, nitrate, ammonium, and chloride, whose mass concentrations were calculated from the intensities of characteristic ionic fragments detected by the mass spectrometer. RIEs were not specifically calibrated for individual organic compounds or dye-related fragments; instead, standard RIE values commonly used in HR-ToF-AMS studies were employed. This approach aligns with the primary goal of this study, which is to analyse the relative temporal variability and compositional changes of fine particulate matter during a fireworks-related pollution event, rather than to determine the exact mass of individual organic species (Zhang et al., 2019).Fireworks emissions comprise a

complex mixture of organic compounds, including dyes, binders, and combustion by-products, for which compound-specific RIE calibrations are generally unavailable. Consequently, high-resolution organic fragment signals in this study should primarily be seen as relative indicators of source influence and aerosol evolution, rather than precise quantifications of mass. Typically, we employed the default RIE value of 1.4 for total organics, suitable for typical ambient oxidized conditions (Zhang et al., 2019). Additionally, we used the default RIE values of 1.1 for nitrate, 1.2 for sulphate, and 1.3 for chloride.

Although the HR-ToF-AMS detects only positively charged ions from electron impact ionization (e.g., NO_2^+, SO^+, $C_xH_y^+$), reported concentrations refer to the parent neutral species in the aerosol. This approach aims to quantify particulate-phase chemical composition, not the ionic forms produced during ionization. Species are reconstructed using known fragmentation patterns and calibration factors. For example, nitrate (NO_3) is measured from NO_2^+ and NO_3^+ signals, sulphate (SO_4) from fragments like SO^+, SO_2^+, SO_3^+, and HSO_3^+. Organic aerosol (ORG) is derived from hydrocarbon and oxygenated ion fragments (e.g., $C_xH_y^+$ and $C_xH_yO_z^+$). This method allows quantification of major aerosol species: ORG, NO_3, SO_4, and NH_4, Cl.

The elemental composition of the Organic Aerosol (OA) was determined using the calibration factors reported in (Canagaratna et al., 2015). This included calculating hydrogen-to-carbon (H:C) and oxygen-to-carbon (O:C) ratios (Van Krevelen diagram) and the carbon oxidation state (OSc) (Van Krevelen, 1950; Ng et al., 2010, 2011). The OSc provides valuable insights into the degree of oxidation of OA species, reflecting their atmospheric aging and processing (Kroll et al., 2011). A more comprehensive explanation of the data processing methodology and the derived informational content from the HR-ToF-AMS is available in (Sasso et al., 2024).

In addition to the mass spectrometry data, Particle Time-of-Flight (P-ToF) analysis was employed to determine the aerodynamic size distributions of the aerosol particles. The P-ToF mode enables characterisation of particles by physical size, providing complementary information

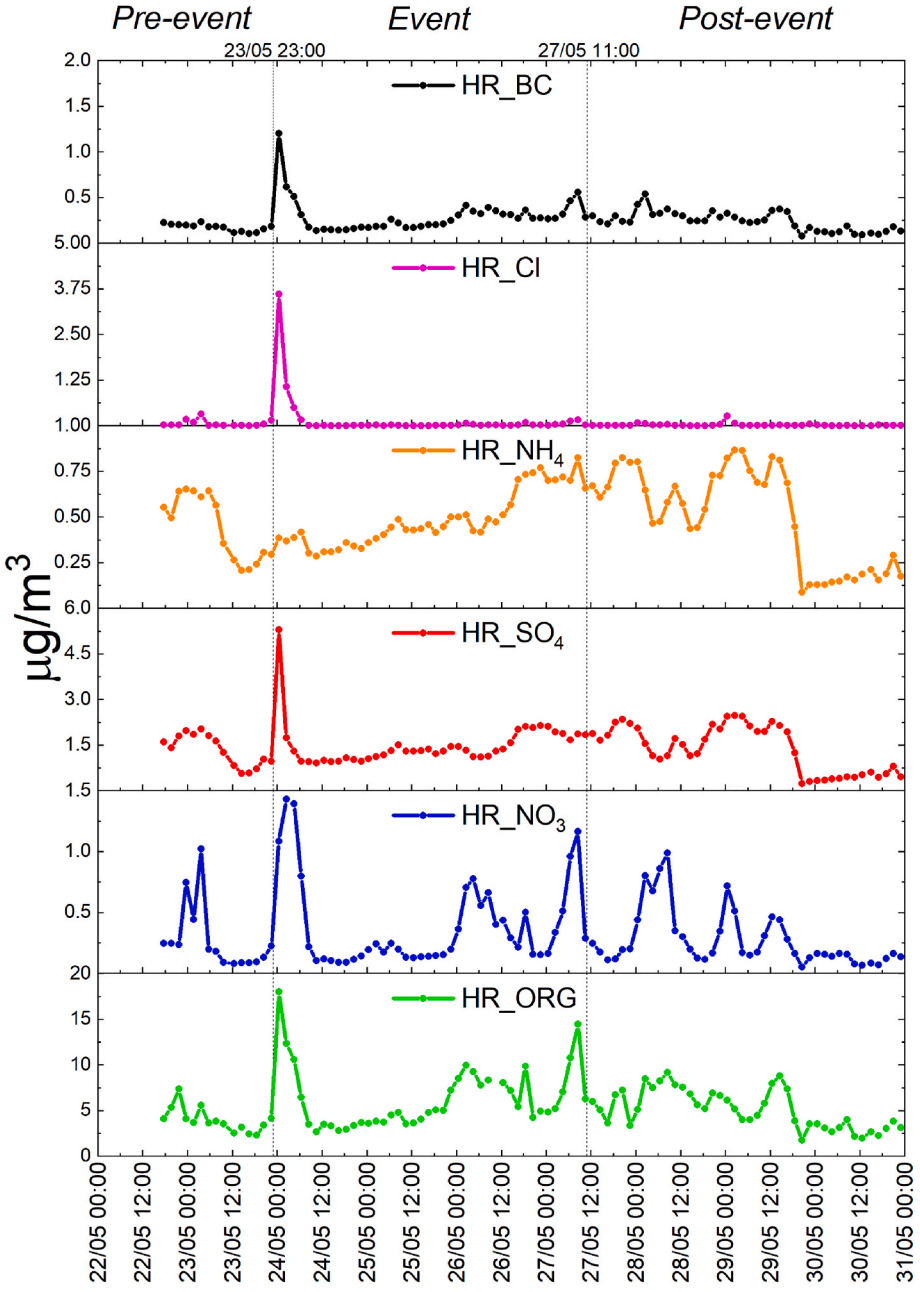

Fig. 2. Time series of main aerosol chemical components subdivided into the three main time periods: pre-event, event, and post-event.

to the chemical composition obtained in the MS mode. The distributions were typically presented as dM/dlogDa, representing the mass concentration (M) per logarithmic interval of aerodynamic diameter (Da), allowing for a clear visualization of how aerosol mass is distributed across different size ranges (Jayne et al., 2000).

3. Discussion and results

The study investigates the impact of celebratory events on atmospheric chemistry and air quality in Naples from the afternoon of May 22nd to May 31st, 2025. The monitoring period was segmented into three phases: *pre-event*, *event*, and *post-event*. The main celebration took place from 11:00 p.m. on 23 May to 5:00 a.m. on May 24, 2025, which is referred to as *celebration night.* The *event* phase encompasses the period from the *celebration night* to the morning of 26th May, during which a secondary, more localized celebration took place in a specific part of the city, approximately 10 km from the acquisition site.

3.1. Time series analysis

The high-resolution time series, shown in Fig. 2, captures the dynamic response of atmospheric aerosol concentrations during the analysed period. The primary aerosol species (ORG, NO_3, SO_4, NH_4, Cl, and BC, derived from SP-AMS) were monitored continuously. Concentrations during the *pre-event* phase (22–23 May) provide a reference level, followed by a pronounced spike across multiple components during the night of 23 May. During the *post-event* period (28–31 May), total aerosol concentrations decreased toward values comparable to the *pre-event*, although remaining slightly elevated. A persistent shift in aerosol chemical composition was also detected in the days following the main event, indicating the prolonged influence of pyrotechnic emissions rather than a permanent change in atmospheric conditions.

Before the *event,* submicron aerosol was primarily composed of typical urban background species: oxidized organic matter dominated, with secondary contributions from NO_3 and SO_4 species, along with moderate levels of NH_4 and BC, likely originating from vehicular traffic and other routine emissions. Chloride concentrations were negligible during this *pre-event* phase.

During the *celebration night* (23–24 May), all measured species increased sharply, most prominently ORG, Cl, and NO_3, as reported in Fig. 2. ORG concentrations reached levels several times larger than those observed during the *pre-event*, reflecting intense emissions from firework combustion and smoke bombs, both of which are rich in organic carbon and soot. A distinct rise in chloride-containing particles was also observed, transitioning from near-zero values to comprising a substantial fraction of total aerosol mass. This signature is characteristic of fireworks, which often include chlorine-rich oxidizers (e.g., potassium chlorate and perchlorate) that generate gaseous HCl and particulate KCl upon detonation (Liu et al., 1997; Perry, 1999; Kulshrestha et al., 2004; Drewnick et al., 2006b; Dutcher et al., 1999). Similarly, NO_3 concentrations increased significantly during the event, consistent with the use of nitrate-based oxidants, such as potassium nitrate (KNO_3), and the subsequent formation of nitrate aerosols from nitrogen oxide emissions (Wang et al., 2007b). SO_4 levels increased more modestly, likely due to the presence of sulphur-containing compounds in firework formulations (Chhabra et al., 2020). NH_4 concentrations remained largely unaffected by the event and showed weaker temporal correlation with the other main aerosol components, consistent with previous studies (Drewnick et al., 2006b). BC concentration roughly doubled during peak celebration hours, indicating a large influx of soot and elemental carbon from pyrotechnic devices, flares, and the traffic contribution. Collectively, these observations suggest a transformation in aerosol concentration during the event, from a relatively stable, secondary-dominated background to a chemically diverse, highly primary aerosol dominated by firework- and flare-related emissions.

3.2. ARPAC comparison

High-temporal-resolution data from the AMS and daily PM2.5 measurements from the Regional Environmental Protection Agency (ARPAC) monitoring station NA07, located approximately 3 km from CeSMA, both captured the impact of the celebration. As shown in Fig. 3, the average bi-hourly concentrations of AMS-derived PM2.5 (calculated as the sum of non-refractory and refractory components transmitted through the PM2.5 lens system) exhibited a pronounced and short-lived increase during the night of 23–24 May, driven by fireworks emissions, combustion sources, and vehicular traffic associated with the celebrations. The PM2.5 peak observed by the AMS aligns with the daily enhancement recorded by the ARPAC network, confirming that both sampling points captured the same pollution episode. However, differences in spatial representativeness (e.g., a 3 km separation and distinct local source environments) and temporal resolution (sub-hourly vs. daily averages) preclude a direct quantitative mass balance. The higher magnitudes observed at the CeSMA site likely reflect a near-source effect or the interception of a more intense portion of the fireworks plume, introducing a potential spatial bias. Consequently, the comparison is intended to provide contextual support for the timing and intensity of the event rather than a point-to-point validation of absolute concentrations.

To contextualize the magnitude of the observed episode within typical fireworks-driven pollution in Naples, the Scudetto celebration was compared with the New Year's Eve 2025 event using PM2.5 observations from the ARPAC Campania monitoring network. New Year's Eve fireworks are known to produce the most intense short-term perturbations of fine particulate matter in the city. During the 2025 New Year period, daily average PM2.5 concentrations increased from background levels of 29 and 42 μg m^{-3} on 29 and 30 December to about 91 and 97 μg m^{-3} on 31 December and 1 January, followed by a rapid decrease within the subsequent two days,2 and 3 January, to values of approximately 34 and 7 μg m^{-3}. Both the New Year's Eve and Scudetto events were therefore characterized by sharp and short-lived PM2.5 peaks rather than sustained multi-day mass enhancements.

Although absolute PM2.5 concentrations during the Scudetto celebration were moderate compared to typical wintertime fireworks events, the relative increase with respect to the local pre-event background was substantial, reflecting the strong perturbation induced by fireworks emissions under late-spring background conditions and during the Scudetto celebrations.

However, despite the rapid recovery of PM2.5 concentrations after the Scudetto celebration, the chemically resolved AMS measurements revealed a slower return of aerosol chemical composition toward pre-event conditions. Changes in the oxidation state of organic aerosol and in the relative contributions of major aerosol components persisted beyond the main PM2.5 peak, indicating a decoupling between mass concentration and chemical recovery. This highlights that, while regulatory PM2.5 metrics capture the intensity of fireworks-driven pollution, chemically resolved measurements are required to fully characterize the atmospheric impact of such episodic urban events.

3.3. Aerosol chemical composition

In addition to variations in aggregate concentrations, the episode left behind specific chemical signatures. In the following section, we analyse the characteristic tracers of pyrotechnic emissions.

Fig. 4 reports the changes in aerosol composition associated with the combustion products released during the celebrations. The figure presents histogram-based averaged concentrations of the main aerosol species across the four time periods: *pre-event*, *event*, *post-event,* and the *celebration night*. The analysis showed a rapid and pronounced increase in multiple main aerosol constituents during the celebration window, consistent with the time series presented in Fig. 2. The presence of these species highlights the influence of celebration-related emissions on the

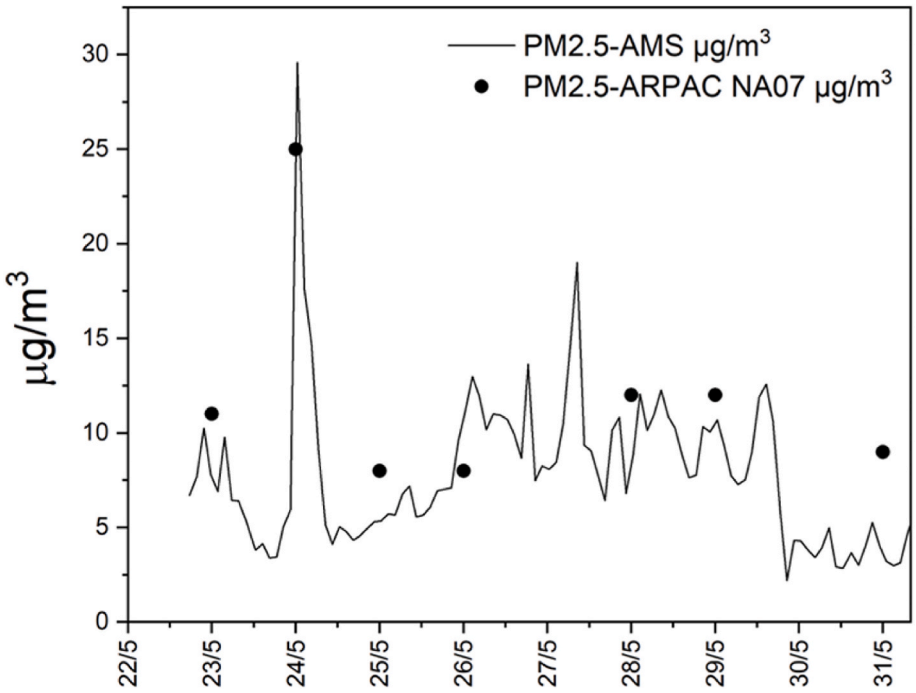

Fig. 3. Time series of PM2.5 concentrations measured by the HR-ToF-AMS (hourly averages, solid line) and daily average PM2.5 concentrations from the ARPAC monitoring station NA07 (black dots), located approximately 3 km from the measurement site.

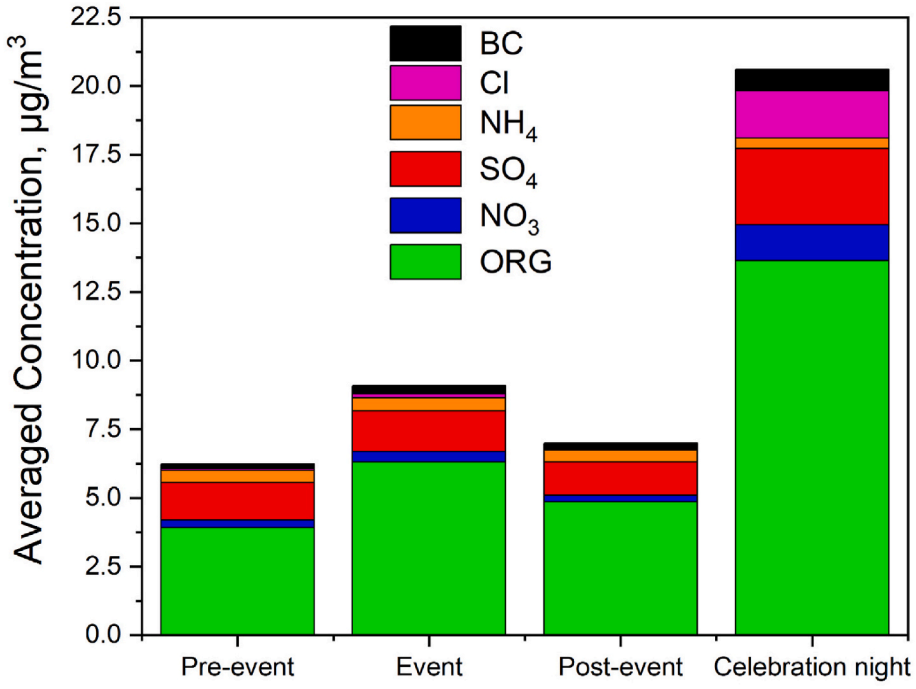

Fig. 4. Histogram representation of the main chemical compound (µg m^{-3}) concentration during the period analysed.

atmospheric aerosol burden during the event peak.

High-resolution analysis enabled a detailed understanding of the aerosol's chemical composition across the measured phases. The fitted ions in the high-resolution region were grouped based on their molecular composition in nine families: C_x, CH, CHO_1, CHO_{gt1} (for number of oxygen atoms greater than one), CHN, NH, Cl, NO, and SO, allowing for a deeper understanding of the chemical nature of the aerosol. Fig. 5 presents pie charts illustrating the relative compositional fractions, i.e., the percentage contribution of an ion family to the total aerosol mass for each measurement, and thus the variation in aerosol chemical composition across the four time periods.

During the *pre-event* period, the aerosol composition was dominated by the CH (29.6%) and CHOgt1 (17.9%) families, indicating a background typical of urban, oxidized OA. The significant presence of NH fragments (23.2%) is also indicative of either ammonium-containing organics or background nitrogen species. Contributions from sulphate (SO, 11%), CHO_1 (10.1%), and nitrate (NO_3, 3.4%) could suggest the presence of a mixture of secondary aerosol components (Seinfeld and

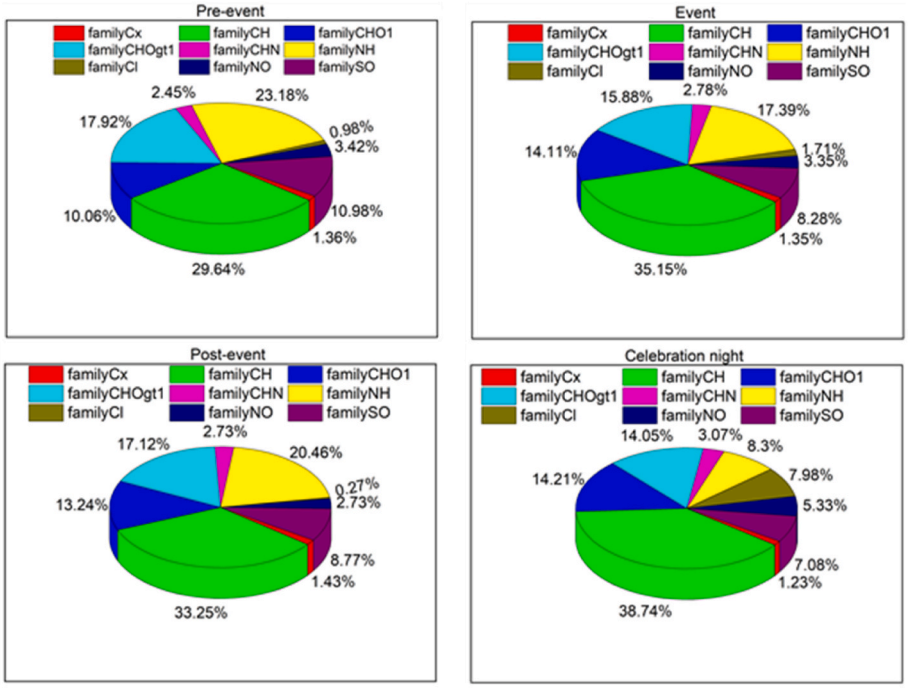

Fig. 5. Pie charts of relative ion family contributions (%). Chemical distribution of the atmospheric aerosol based on the main chemistry families in high-resolution mode. Starting in a clockwise direction from the top-left for: pre-event, event, post-event, and celebration night.

Pandis, 2016; Jimenez et al., 2003; Zhang et al., 2007). Notably, the concentration of chlorine-containing species (Cl) was minimal at 0.98%, consistent with the absence of halogenated emissions in the area, although the measurement point is close to the sea.

During the event phase, noticeable changes occurred in the composition. The CH fraction has increased sharply to 35.1%, indicating an increase in fresh, hydrocarbon-like organics, most likely originating from combustion sources such as fireworks and smoke bombs (Zhang et al., 2005; Zhu et al., 2021). Although the total mass of NH fragments has increased, their relative contribution has decreased to 17.4%, suggesting dilution by a broader range of organic species. The Cl signal rose to 1.7%, an index of pyrotechnic activity. Interestingly, CHO_1 levels increased, whereas CHOgt1 levels did not, even though both increased in absolute terms. This suggests a mixture of fresh and aged material relative to the onset of firework emissions mixed with urban background aerosol.

In the *post-event* phase, although the species' mass concentration had returned to nearly the *pre-event* level, the aerosol composition continued to reflect the event's persistent effects. The CH signal remained high at 33.3%, and both CHO_1 and CHOgt1 stayed elevated. Specifically, CHOgt1 returned to almost its initial level, while CHO1 remained higher. Meanwhile, the NH fraction increased again to 20.5%, whereas Cl and NO decreased notably to 0.27% and 2.73%, respectively. This suggested that the more reactive components of the fireworks emissions had dispersed and that the aerosol was transitioning back towards its *pre-event* chemical state. SO_4 remained stable, indicating that regional secondary sources continued to influence the aerosol composition.

The most distinct and chemically unique profile was observed during the *celebration night*. Within a few hours, the aerosol became heavily enriched in CH (38.7%), indicating the presence of significant amounts of fresh hydrocarbon fragments resulting from intense pyrotechnic activity. In contrast to the broader event phase, NH dropped to 8.3%, indicating that other primary emissions (CH, Cl) dominated the chemical signature at the peak of the fireworks display. Notably, Cl increased significantly to 7.98%, indicating a substantial release of chlorine-containing particles from the fireworks. NO and CHO_1 also increased (to 5.3% and 14.2%, respectively), while CHOgt1 remained elevated at 14%, indicating oxidation or secondary formation, even in the short term (Zhang et al., 2005; Heringa et al., 2012). This analysis confirms the significant impact of the celebrations on atmospheric composition, particularly through short-term bursts of combustion products and coloured smoke emissions.

Fig. 5 illustrates the phase-dependent evolution of aerosol composition through a pie-chart representation of the nine HR ion families, where percentages sum to 100% by construction. *Pre-event* aerosol was dominated by CH (29.6%) and CHOgt1 (17.9%), while celebration night showed elevated CH (38.7%) and Cl (7.98%) with reduced NH (8.3%). To assess the robustness of these compositional shifts, we also examined the mass contributions and their intra-phase variability from hourly measurements (Table 1). The CH family increased from 2.28 μg m^{-3} *pre-event* to 6.90 μg m^{-3} during *celebration night,* while chloride rose from 0.08 μg m^{-3} to 1.42 μg m^{-3}. These changes substantially exceed intra-phase standard deviations, confirming that the pie-chart shifts reflect statistically significant pyrotechnic influence.

Table 1
Contribution of the main chemistry families to the total aerosol mass measured during the four defined phases: Pre-event, event, Post-event, and the Celebration night.

	Pre-Event,$\mu g\ m^{-3}$	Event,$\mu g\ m^{-3}$	Post-Event,$\mu g\ m^{-3}$	Celebration night, $\mu g\ m^{-3}$
Family Cx	0.104	0.151	0.124	0.219
Family CH	2.276	3.930	2.918	6.897
Family CHO1	0.772	1.578	1.149	2.530
Family CHOgt1	1.376	1.776	1.486	2.502
Family CHN	0.188	0.311	0.237	0.546
Family NH	1.780	1.945	1.775	1.478
Family Cl	0.076	0.191	0.023	1.421
Family NO	0.262	0.375	0.237	0.948
Family SO	0.843	0.926	0.761	1.260

3.4. Characteristics of tracers in HR-ToF-AMS

Chemical tracers of pyrotechnic activities include key fuel materials (charcoal, sulphur) and the primary oxidizers (potassium nitrate, chlorate, and perchlorate) (Wang et al., 2007a; Liu et al., 1997; Perry, 1999; Kulshrestha et al., 2004; Drewnick et al., 2006b; Dutcher et al., 1999). In addition to monitoring Cl, NO_3, and SO_4 fragments, as previously discussed, the presence of metals typically responsible for the characteristic colours of fireworks has been examined. Fig. 6 presents the temporal concentration profiles of Ba, Sr, and Cu, associated with green, red, and blue colours, respectively (Webster, 1985; Steinhauser et al., 2008). Although their absolute concentrations were extremely low, a notable and sudden spike in all three metals coincided precisely with the onset of the celebrations. The timing of this signal suggests an immediate and direct atmospheric response to pyrotechnic emissions.

Smoke bombs are composed of tailored chemical mixtures designed to produce distinct visual effects, particularly through coloured smoke. These formulations typically include an oxidising agent such as potassium chlorate, a fuel like lactose or dextrin, and a powdered organic dye that determines the colour of the emitted smoke (Fathollahi et al., 2004; Eslami and Hosseini, 2011). Specific molecular species were monitored using HR-ToF-AMS high-resolution *m/z* ratios. Figs. 7 and 8 illustrate the temporal evolution of representative fuel-related compounds and dye molecules. Fig. 7 illustrates the time-resolved concentration profiles of the disaccharide Lactose ($C_{12}H_{22}O_{11}$) and the monosaccharide Glucose ($C_6H_{12}O_6$). The simultaneous presence of these two compounds is attributed to the thermal decomposition of lactose, a primary fuel component in the pyrotechnic composition (Eslami and Hosseini, 2011). The increase in glucose concentration temporally aligns with the increase in lactose concentration, suggesting that glucose is a key fragmentation product generated during the high-temperature vaporization of lactose in the HR-ToF-AMS or during the pyrotechnic reaction itself.

Fig. 8 presents the temporal evolution of the most probable molecular fragments for the primary pyrotechnic dyes. The analysis focused on those associated with light blue (Indigo, $C_{16}H_{10}N_2O_2$), red (a mixture of α-methoxybenzenazo-β-naphthol, *Red 1*, $C_{17}H_{14}N_2O_2$; and 1,4-diamino-2-methoxyanthraquinone, *Red 11*, $C_{15}H_{12}N_2O_3$), and green (a mixture of 1,4-diphenyl-9,10-anthraquinone, *Green 3*, $C_{28}H_{22}N_2O_2$; and 2-(2-quinolinyl)-1,3-indandione, *Yellow 33*, $C_{18}H_{11}NO_2$) smoke compositions. (Harriman, 2025; Toxicity of Military Smokes and, 1999). The rapid and synchronized increase in fragment concentration confirms their direct source from the pyrotechnic event, and their decomposition contributes

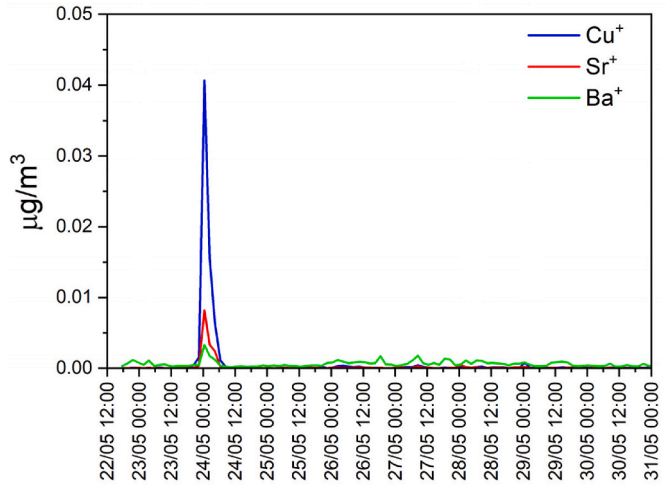

Fig. 6. Time series of the metals responsible for coloured light in the fireworks. The time series of Cu, Sr, and Ba metal ions were reported in blue, red, and green, respectively. (For interpretation of the references to colour in this figure legend, the reader is referred to the Web version of this article.)

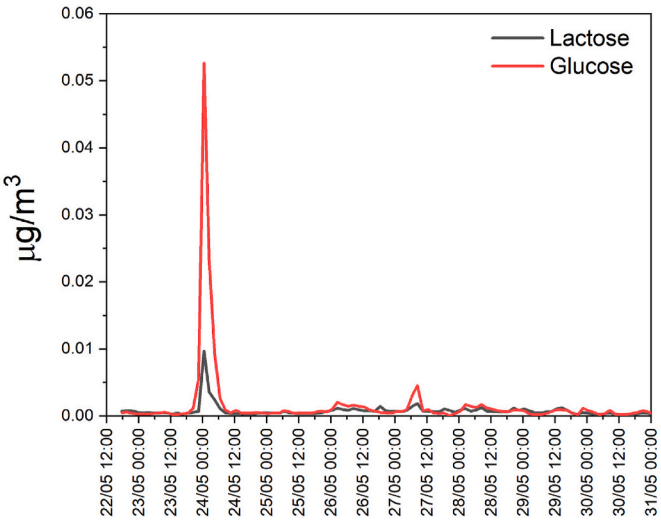

Fig. 7. Time series of lactose ($C_{12}H_{22}O_{11}$) and glucose ($C_6H_{12}O_6$) molecules.

to the overall rise in CH fragments observed in the OA composition (see Fig. 6). The inset visualizes the hypothesized bond breakage points for each dye molecule.

Because several trace-level markers (including Ba^+, Sr^+, Cu^+ and selected organic and oxidant-related signals) are close to the instrumental detection limit, their absolute mass concentrations are affected by relatively large uncertainties. These time series are therefore interpreted primarily as qualitative temporal tracers of pyrotechnic activity, focusing on timing and relative enhancement rather than on precise quantitative mass estimates.

3.5. Elemental analysis and carbon oxidation state

Elemental analysis of atmospheric aerosol was performed using the high-resolution mode of the HR-ToF-MS. Fig. 9 presents the Van Krevelen diagram, including all H:C vs. O:C data acquired during the sampling period. On the plot, the data points are represented as follows: *pre-event* (black squares), *event* (full red dots), *celebration night* (lower cyan triangles), and *post-event* (upper green triangles). Due to the wide dispersion of data points across the plot, a clear temporal ageing trend is difficult to discern visually. The data generally fall between the "alcohol/peroxide" and "carboxylic acid" pathways, which suggests the observed OA is undergoing complex atmospheric aging involving various functionalization reactions that simultaneously alter the H:C and O:C ratios (Canagaratna et al., 2015; Ng et al., 2010, 2011). To provide a more quantitative assessment of the chemical evolution, Table 2 summarizes the mean H:C, O:C, and OSc values for each sampling period.

In *pre-event* phase, the OA exhibited an average O:C ratio of approximately 0.603 and an H:C ratio near 1.500. This composition is indicative of a relatively oxidized, aged OA, characteristic of urban Secondary Organic Aerosol (SOA). During the *event*, the O:C ratio declined to ~0.563, while the H:C ratio increased slightly. This effect was even more pronounced during the *celebration night*, where the O:C value decreased further and the H:C value increased even more. In the *post-event*, this trend persisted: O:C remained lower at ~0.553, and H:C remained marginally elevated relative to *pre-event* conditions. These changes in Van Krevelen space, a decrease in O:C accompanied by a modest increase in H:C, is contrary to the typical trajectory associated with atmospheric aging, where oxidation generally increases O:C and reduces H:C. Instead, this trend reflects the introduction of fresher, more reduced organic material with fewer oxygen-containing functional groups and relatively greater hydrogen content, in agreement with the trend shown in Fig. 5. These changes strongly suggest the emission of

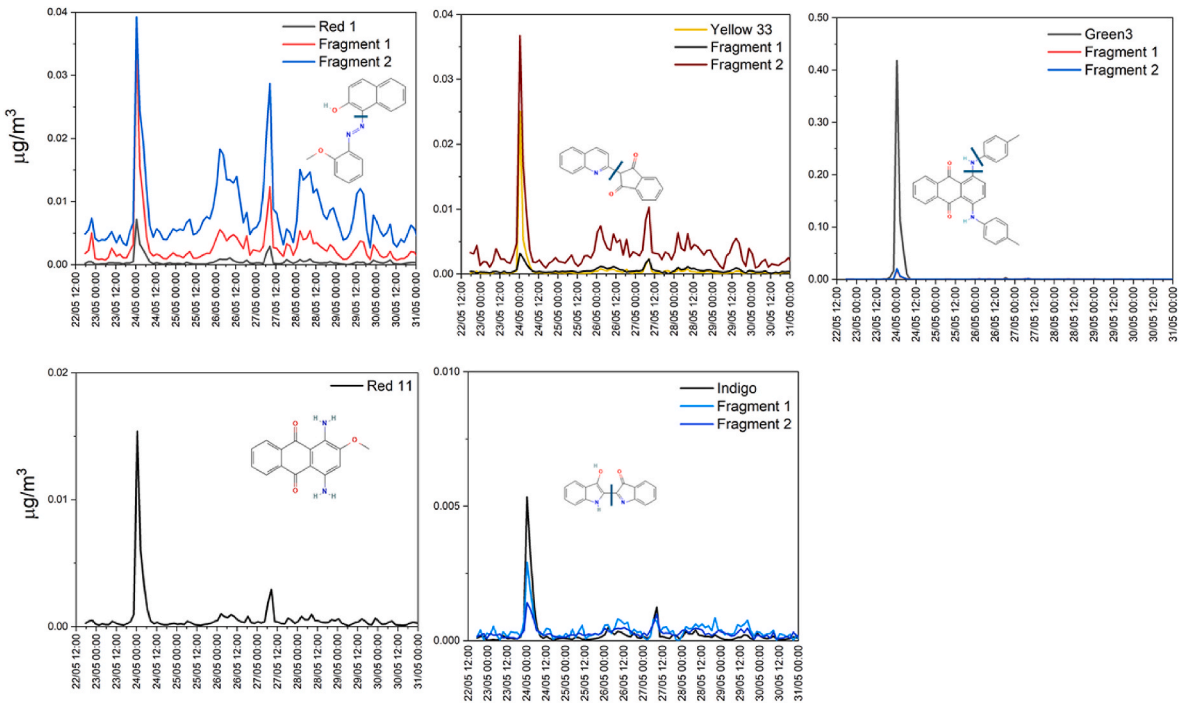

Fig. 8. Time-resolved mass concentrations and fragmentation analysis of key dye compounds detected during the event (Indigo-light blue, MBN-Red 1, DMA-Red 11, PTA-green 3, and QID-Yellow 33). (For interpretation of the references to colour in this figure legend, the reader is referred to the Web version of this article.)

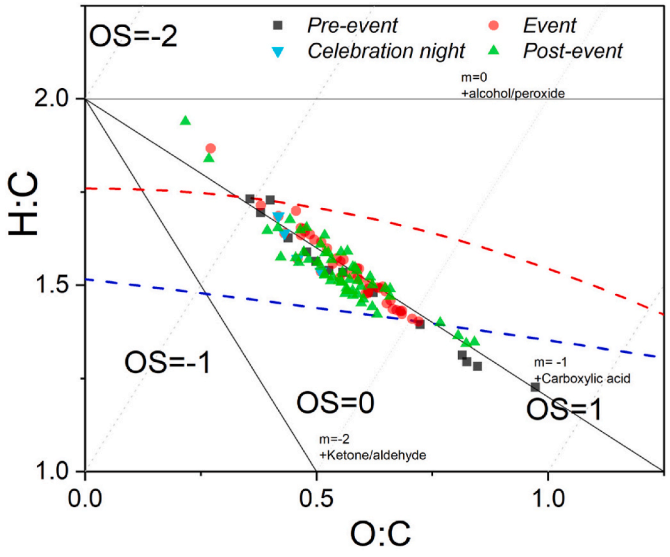

Fig. 9. Van Krevelen diagram reporting the H:C vs. O:C elemental ratios for the entire analysis period. The data points are categorized by sampling period: pre-event (black squares), event (full red dots), celebration night (lower cyan triangles), and post-event (upper green triangles). Black solid lines, labeled m, demarcate regions associated with key oxygenated functional groups. The positive-slope grey dashed lines indicate various OSc. The blue and red dashed lines represent the lower and upper boundaries of the region where typical ambient OA samples are generally found. (For interpretation of the references to colour in this figure legend, the reader is referred to the Web version of this article.)

primary combustion aerosols during the event, likely from fireworks and flares. The initially higher pre-event O:C value reflects the dominance of aged, oxidized SOA. In contrast, the lower O:C (~0.45) observed during the celebration points to the presence of freshly emitted, less oxygenated organics. The continued suppression of O:C after the event, along with

Table 2
Averaged values of H:C and O:C elemental ratios and OSC for the entire analysis period.

	Average O:C	Average H:C	Average OSc
Pre-event	0.603 ± 0.014	1.500 ± 0.012	−0.294 ± 0.041
Event	0.563 ± 0.002	1.546 ± 0.002	−0.420 ± 0.007
Post-event	0.553 ± 0.002	1.539 ± 0.002	−0.434 ± 0.006
Celebration night	0.454 ± 0.007	1.608 ± 0.019	−0.700 ± 0.033

sustained higher H:C, implies a lingering influence from these primary emissions, whether due to slow oxidation of introduced material or the persistence of residual primary particles.

The average carbon OSc was calculated to analyse the observed compositional changes in the OA across the study period. As a key metric of aerosol aging, OSc quantifies the average oxidation level of organic components. (Kroll et al., 2011). In *pre-event*, the mean OSc was approximately −0.294, indicating a moderately oxidized urban background aerosol. This slightly negative value indicates a mixture of oxidized and reduced species. Following the *event*, the aerosol population was less oxidized and more hydrogen-rich, with a correspondingly lower average OSc. This shift is consistent with an influx of new, primary emissions or a temporary reduction in photochemical processing, leaving the *post-event* aerosol in a more reduced state relative to the *pre-event* background.

3.6. Particle size distribution analysis

Having examined the chemistry, we will proceed to evaluate the particle size distribution and the consistency of the instruments' readings.

Atmospheric aerosol particle size distributions (PSDs) during the celebrations were characterized using an HR-ToF-AMS in P-ToF mode and an OPS. This dual-instrument approach enabled a combined assessment of submicron chemically resolved aerosol (AMS, including SP-AMS refractory components) and total particle number concentration up to 10 µm (OPS), allowing direct comparison of mass and number-

based metrics. The OPS particle number-size distribution (dN/dLogDp, #/cm^3 vs. Dp, *nm*) (Fig. 10) provides a complementary view, extending the particle-size analysis beyond the typical AMS detection limit. The *pre-event* number curve (black squares) reflects typical urban background conditions, with a submicron number concentration (approximately 130 #/cm^3 at 337 nm, declining to approximately 0.02 *#/cm^3* at about 10000 nm). Conversely, *during the event* (red circles), and particularly on the *celebration night* (cyan down-triangles), a marked increase in particle number is observed across nearly all size ranges, with the strongest enhancement below 1000 nm. This broad increase is consistent with intense pyrotechnic combustion and rapid formation of fresh primary particles from fireworks and smoke bombs. *Post-event* (green up-triangles), number concentrations returned to *pre-event* period while the 400–1000 nm range exhibited relative depletion, and the coarse-mode number remained elevated. This behaviour suggests size-dependent removal mechanisms, with accumulation-mode particles being preferentially diluted, while coarse particles persist longer in the lower atmosphere. At the same time, aerosol chemical composition continued to exhibit pyrotechnic signatures, indicating a temporal decoupling between particle number recovery and chemical perturbation.

This key distinction will become further apparent through the complementary AMS-OPS mass distribution analysis. Indeed, to enable a direct comparison, the OPS number PSDs were converted into an equivalent mass PSD (dM/dLogDp, *μg m^{-3}*). Given the absence of direct measurements of aerosol effective density during the sampling period, a uniform effective density of $\rho_{eff} = 1.4$ g cm^{-3} was assumed and applied to the OPS number data for this number-to-mass conversion. This value is characteristic of internally mixed, aged urban aerosols, reflecting a moderate degree of oxidation and a chemical composition dominated by the organic fraction (Rissler et al., 2014; Cross et al., 2007). Regarding the OPS-derived mass, it is important to consider the uncertainty linked to the fixed density assumption. Pyrotechnic particles, often composed of heavy metal salts or fractal soot, can exhibit densities that deviate from standard urban values. However, sensitivity considerations suggest that, although the choice of ρ_{eff} linearly scales absolute mass concentrations, it does not affect the qualitative interpretation of the event, such as the timing of the peaks or the relative prominence of observed size modes.

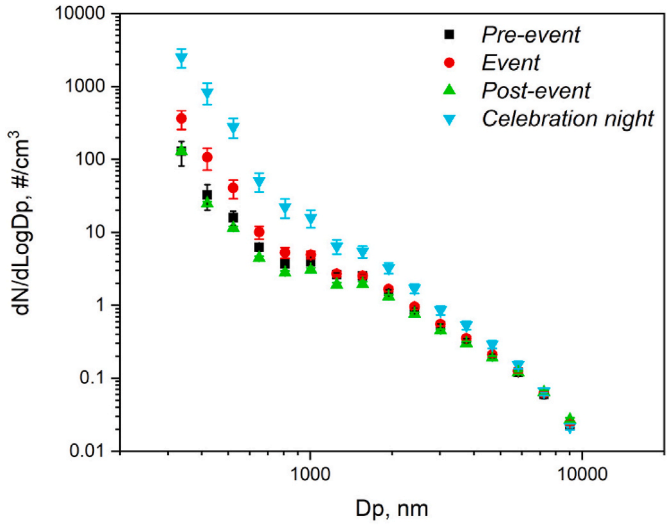

Fig. 10. PM number size distribution. The four curves represent the four time periods analysed. The curve with a black square represents the distribution before the event; the red circle represents the distribution during the celebration period; the green triangles represent the distribution after the event; the cyan diamonds represent the distribution during the celebration night. (For interpretation of the references to colour in this figure legend, the reader is referred to the Web version of this article.)

The size-resolved mass distributions from AMS and OPS (presented in Fig. 11) show distinct, phase-dependent patterns that reflect differences in aerosol composition, morphology, and instrument response. Instead of a perfect overlap across all sizes, the two instruments exhibit systematic divergences that are physically interpretable and highlight their complementary capabilities. During the *pre-event*, *event*, and *post-event* periods, the AMS mass distribution is dominated by an accumulation-mode peak at ~550–700 nm, while the OPS displays a broader distribution including substantial coarse-mode mass around 5–6 μm. In the 300–1250 nm range, the OPS-derived mass is typically lower than that of AMS, whereas above ~1250 nm, the OPS reports higher mass due to its sensitivity to coarse particles. These differences arise from the distinct detection approaches of the two techniques: aerodynamic focusing and flash vaporization for the AMS versus optical sizing combined with density conversion for the OPS. The gradual decrease in the AMS signal with increasing diameter reflects the expected decline in the transmission efficiency of the PM2.5 aerodynamic lens, whereas the OPS fully captures large refractory particles. The comparison in this overlap region is therefore interpretative rather than a test of quantitative closure.

The *celebration night* exhibits a fundamentally different and more complex behaviour. Most strikingly, at the finest measured size (nominally 337 nm for OPS), an acute spike is observed where OPS reports ~50.7 μg m^{-3}, while the AMS at a comparable aerodynamic diameter measures ~5.6 μg m^{-3}. While this feature likely reflects a genuine and intense production of submicron particles from smoke-bomb combustion, its absolute magnitude must be interpreted with caution. At this size bin, OPS optical sizing is based on Mie theory and a default refractive index; the presence of highly absorbing, non-spherical, or dye-rich particles, typical of pyrotechnic emissions, can significantly bias the optical-equivalent diameter and the subsequent mass conversion. Therefore, this spike is interpreted as a qualitative indicator of extreme fine-particle loading rather than a precise physical mass measurement. Beyond the acute 337 nm feature, which likely represents an upper-bound estimate due to the aforementioned optical uncertainties, the OPS and AMS signals converge progressively as size increases up to 1250 nm. Throughout this intermediate range, the two instruments report increasingly similar mass concentrations, indicating that the intense organic loading from smoke bombs has saturated the metal-core particles with organics, and the resulting swollen, organic-enriched particles are now equally visible to both AMS and OPS. The AMS maintains its characteristic accumulation-mode peak at approximately 700 nm, with a maximum intensity of roughly 8 μg m^{-3}. In contrast, the OPS contribution in the 300-1250 nm range rises to comparable values.

Above 1250 nm, the pattern reverts to the relationship observed in earlier phases, with OPS again exceeding AMS, now reaching a maximum intensity of approximately 16.5 μg m^{-3} at approximately 5000 nm. This coarse-mode enhancement observed on the night of the celebration reflects direct, continuous large-particle emission from active pyrotechnic devices throughout the celebration.

Overall, the phase-dependent AMS–OPS behaviour highlights the complementarity of the two instruments and demonstrates that the event generated a complex, multimodal aerosol burden spanning freshly formed submicron particles, an enhanced accumulation mode, and a substantial coarse refractory fraction.

This integrated perspective reveals that PM2.5 regulatory metrics alone would substantially underestimate both the acute exposures during peak pyrotechnic emissions (via the 337 nm spike) and the lingering coarse-mode burden (via the 5000 nm plateau), with implications for exposure assessment, air quality forecasting, and source apportionment studies targeting episodic events in urban environments.

4. Conclusions

Combined monitoring of particulate matter using HR-ToF-AMS and

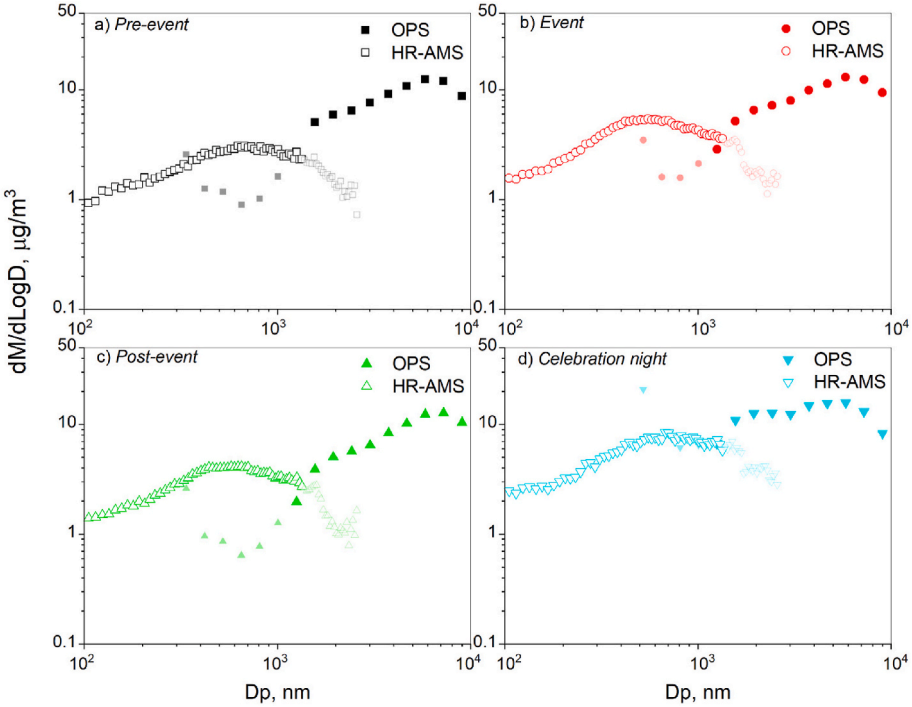

Fig. 11. Aerosol mass size distributions, presented as dM/dLogDp (µg m^{-3}), for the four distinct time periods analysed. The open symbols represent data collected by the HR-ToF-AMS, while the filled symbols represent data from the converted OPS. Partially transparent symbols denote the size region where AMS and OPS measurements overlap; differences in this range arise from the distinct detection principles, size-dependent transmission efficiency of the AMS, and the assumed effective density used for the OPS mass conversion. The comparison in this region is therefore interpreted qualitatively. The four panels track the evolution of the particle mass distribution: (a) Pre-event (black squares/open squares). (b) Event (red circles/open circles). (c) Post-event (green triangles/open triangles). (d) Celebration night: (cyan diamonds/open diamonds). The figure clearly illustrates the change in particle-size mode, particularly the increase in the coarse-mode mass during the event periods, as captured by the OPS data. (For interpretation of the references to colour in this figure legend, the reader is referred to the Web version of this article.)

OPS during sports victory celebrations revealed a significantly variable, chemically complex aerosol load in the urban atmosphere. The measurements show a marked increase in aerosol concentrations on the celebration night, with particles enriched in organic compounds of pyrotechnic origin, trace metals (Ba, Sr, Cu), and chloride. High-resolution analysis indicates the introduction of fresh organic carbon, with increasing H:C and decreasing O:C ratios, along with increased contributions of nitrate and chloride, consistent with characteristics of fireworks emissions. The temporal profile indicates that the pollution peak occurred overnight during the celebration, followed by a gradual decrease to levels comparable to those in the *pre-event* period, although chemical signatures of primary species persisted for several days. This behaviour indicates that, unlike a brief fireworks display, a prolonged pyrotechnic event can produce extended chemical perturbations even after particle mass decreases. The increase in particulate mass was primarily in the accumulation mode (submicron particles), as indicated by the AMS, while the OPS detected a marked enhancement in particle number concentrations at the smallest measurable sizes. This result highlights the need to consider both mass (PM2.5) and numerical metrics when describing fireworks emissions: most of the chemically characterized aerosol mass falls below the 2.5 µm threshold, whereas short-lived peaks in fine particle number concentrations may influence near-field exposure conditions even when mass concentrations remain moderate.

In summary, this study demonstrates that such urban pyrotechnic events generate acute, chemically complex pollution episodes that significantly alter the chemical composition and size distribution of aerosols. Although the total mass increase quickly decreases to values within the range observed during the pre-event reference period, the chemical signatures of pyrotechnic compounds persist for several days after the event. Such sports-victory fireworks should therefore be interpreted as episodic atmospheric perturbations superimposed on the broader urban background. Their primary scientific relevance lies in providing a natural experiment for investigating emission signatures, atmospheric processing, and short-term exposure peaks rather than representing persistent air-quality conditions. Overall, these results highlight the limitations of PM2.5-only metrics and emphasize the need for integrated, size- and chemistry-resolved measurements to properly characterize the impact of such episodic urban emission events on air quality and short-term exposure.

CRediT authorship contribution statement

Francesca Picca: Writing – review & editing, Writing – original draft, Investigation, Data curation, Conceptualization. **Fabio Sasso:** Writing – review & editing, Writing – original draft, Investigation, Data curation, Conceptualization. **Andrea D'Anna:** Writing – review & editing, Supervision, Project administration, Data curation.

Declaration of competing interest

The authors declare that they have no known competing financial interests or personal relationships that could have appeared to influence the work reported in this paper.

Acknowledgment

This research has been supported by PER-ACTRIS-IT (Potenziamento della componente italiana della Infrastruttura di Ricerca Aerosol, Clouds, and Trace Gases Research Infrastructure), – Avviso MUR D.D. no. 2595 del 24.12.2019 Piano Stralcio "Ricerca e Innovazione 2015–2017", funded by the European Regional Development Fund –

MIUR (Italian Ministry of University and Research).

Data availability

Data will be made available on request.

References

Allan, J.D., Jimenez, J.L., Williams, P.I., Alfarra, M.R., Jayne, J.T., Coe, H., et al., 2003. Quantitative sampling using an Aerodyne aerosol mass spectrometer 1. Techniques of data interpretation and error analysis. J. Geophys. Res. Atmos. 108 (3).

Baumgardner, D., Kok, G., Raga, G., 2004. Warming of the Arctic lower stratosphere by light absorbing particles. Geophys. Res. Lett. 31 (6).

Canagaratna, M.R., Jayne, J.T., Jimenez, J.L., Allan, J.D., Alfarra, M.R., Zhang, Q., et al., 2007. Chemical and microphysical characterization of ambient aerosols with the aerodyne aerosol mass spectrometer. Mass Spectrom. Rev. 26, 185–222.

Canagaratna, M.R., Jimenez, J.L., Kroll, J.H., Chen, Q., Kessler, S.H., Massoli, P., et al., 2015. Elemental ratio measurements of organic compounds using aerosol mass spectrometry: characterization, improved calibration, and implications. Atmos. Chem. Phys. 15 (1), 253–272.

Cao, X., Zhang, X., Tong, D.Q., Chen, W., Zhang, S., Zhao, H., et al., 2018. Review on physicochemical properties of pollutants released from fireworks: environmental and health effects and prevention. Environ. Rev. 26 (2), 133–155.

Charlson, R.J., Schwartz, S.E., Hales, J.M., Cess, R.D., Coakley, J.A., Hansen, J.E., et al., 1992. Climate forcing by anthropogenic aerosols. Science 255 (5043), 423–430, 1979.

Chhabra, A., Turakhia, T., Sharma, S., Saha, S., Iyer, R., Chauhan, P., 2020. Environmental impacts of fireworks on aerosol characteristics and radiative properties over a mega city, India. City Environ. Interact. 7, 100049.

Cross, E.S., Slowik, J.G., Davidovits, P., Allan, J.D., Worsnop, D.R., Jayne, J.T., et al., 2007. Laboratory and ambient particle density determinations using light scattering in conjunction with aerosol mass spectrometry. Aerosol. Sci. Technol. 41 (4), 343–359.

(CS), 2025. Polveri Sottili in Campania, Cosa È Successo Durante i Festeggiamenti? https://www.arpacampania.it/-/-cs-polveri-sottili-in-campania-cosa-%C3%A8-successo-durante-i-festeggiamenti.

DeCarlo, P.F., Kimmel, J.R., Trimborn, A., Northway, M.J., Jayne, J.T., Aiken, A.C., et al., 2006a. Field-deployable, high-resolution, time-of-flight aerosol mass spectrometer. Anal. Chem. 78 (24), 8281–8289.

DeCarlo, P.F., Kimmel, J.R., Trimborn, A., Northway, M.J., Jayne, J.T., Aiken, A.C., et al., 2006b. Field-deployable, high-resolution, time-of-flight aerosol mass spectrometer. Anal. Chem. 78 (24), 8281–8289.

Drewnick, F., Hings, S.S., DeCarlo, P., Jayne, J.T., Gonin, M., Fuhrer, K., et al., 2005. A new time-of-flight aerosol mass spectrometer (TOF-AMS) - instrument description and first field deployment. Aerosol. Sci. Technol. 39, 637–658.

Drewnick, F., Hings, S.S., Curtius, J., Eerdekens, G., Williams, J., 2006a. Measurement of fine particulate and gas-phase species during the New Year's fireworks 2005 in Mainz, Germany. Atmos. Environ. 40 (23), 4316–4327.

Drewnick, F., Hings, S.S., Curtius, J., Eerdekens, G., Williams, J., 2006b. Measurement of fine particulate and gas-phase species during the New Year's fireworks 2005 in Mainz, Germany. Atmos. Environ. 40 (23), 4316–4327.

Drewnick, F., Hings, S.S., Alfarra, M.R., Prevot, A.S.H., Borrmann, S., 2009. Atmospheric measurement techniques aerosol quantification with the aerodyne aerosol mass spectrometer: detection limits and ionizer background effects. Atmos. Meas. Tech. 2.

Drewnick, F., Diesch, J.M., Faber, P., Borrmann, S., 2015. Aerosol mass spectrometry: particle-vaporizer interactions and their consequences for the measurements. Atmos. Meas. Tech. 8 (9), 3811–3830.

Dutcher, D.D., Perry, K.D., Cahill, T.A., Copeland, S.A., 1999. Effects of indoor pyrotechnic displays on the air quality in the Houston astrodome. J. Air Waste Manage. Assoc. 49 (2), 156–160.

Eslami, A., Hosseini, S.G., 2011. Improving safety performance of lactose-fueled binary pyrotechnic systems of smoke dyes. J. Therm. Anal. Calorim. 104 (2), 671–678.

Faber, P., Drewnick, F., Veres, P.R., Williams, J., Borrmann, S., 2013. Anthropogenic sources of aerosol particles in a football stadium: real-time characterization of emissions from cigarette smoking, cooking, hand flares, and color smoke bombs by high-resolution aerosol mass spectrometry. Atmos. Environ. 77, 1043–1051.

Fathollahi, M., Pourmortazavi, S.M., Hosseini, S.G., 2004. The effect of the particle size of potassium chlorate in pyrotechnic compositions. Combust. Flame 138 (3), 304–306.

Harriman, A., 2025. A perspective on indigo: an iconic colorant. Colorants 4 (2), 12.

Heringa, M.F., Decarlo, P.F., Chirico, R., Tritscher, T., Clairotte, M., Mohr, C., et al., 2012. A new method to discriminate secondary organic aerosols from different sources using high-resolution aerosol mass spectra. Atmos. Chem. Phys. 12 (4), 2189–2203.

Hu, W., Day, D.A., Campuzano-Jost, P., Nault, B.A., Park, T., Lee, T., et al., 2018. Evaluation of the new capture vaporizer for Aerosol Mass Spectrometers (AMS): elemental composition and source apportionment of Organic Aerosols (OA). ACS Earth Space Chem. 2 (4), 410–421.

Huang, X.F., He, L.Y., Xue, L., Sun, T.L., Zeng, L.W., Gong, Z.H., et al., 2012. Highly time-resolved chemical characterization of atmospheric fine particles during 2010 Shanghai World Expo. Atmos. Chem. Phys. 12 (11), 4897–4907.

Intergovernmental Panel on Climate Change (IPCC), 2023. Climate Change 2021 – the Physical Science Basis. Cambridge University Press.

Jayne, J.T., Leard, D.C., Zhang, X., Davidovits, P., Smith, K.A., Kolb, C.E., et al., 2000. Development of an aerosol mass spectrometer for size and composition analysis of submicron particles. Aerosol. Sci. Technol. 33, 49–70.

Jiang, Q., Sun, Y.L., Wang, Z., Yin, Y., 2015. Aerosol composition and sources during the Chinese spring festival: fireworks, secondary aerosol, and holiday effects. Atmos. Chem. Phys. 15 (11), 6023–6034.

Jimenez, J.L., Jayne, J.T., Shi, Q., Kolb, C.E., Worsnop, D.R., Yourshaw, I., et al., 2003. Ambient aerosol sampling using the aerodyne aerosol mass spectrometer. J. Geophys. Res. Atmos. 108 (D7).

Joo, T., Chen, Y., Xu, W., Croteau, P., Canagaratna, M.R., Gao, D., et al., 2021. Evaluation of a new Aerosol Chemical Speciation Monitor (ACSM) system at an urban site in Atlanta, GA: the use of capture vaporizer and PM $_{2.5}$ inlet. ACS Earth Space Chem. 5 (10), 2565–2576.

Kroll, J.H., Donahue, N.M., Jimenez, J.L., Kessler, S.H., Canagaratna, M.R., Wilson, K.R., et al., 2011. Carbon oxidation state as a metric for describing the chemistry of atmospheric organic aerosol. Nat. Chem. 3 (2), 133–139.

Kulshrestha, U.C., Nageswara Rao, T., Azhaguvel, S., Kulshrestha, M.J., 2004. Emissions and accumulation of metals in the atmosphere due to crackers and sparkles during Diwali festival in India. Atmos. Environ. 38 (27), 4421–4425.

Lionetto, M.G., Guascito, M.R., Giordano, M.E., Caricato, R., De Bartolomeo, A.R., Romano, M.P., et al., 2021. Oxidative potential, cytotoxicity, and intracellular oxidative stress generating capacity of pm10: a case study in south of Italy. Atmosphere 12 (4).

Liu, D.Y., Rutherford, D., Kinsey, M., Prather, K.A., 1997. Real-time monitoring of pyrotechnically derived aerosol particles in the troposphere. Anal. Chem. 69 (10), 1808–1814.

Moore, J.X., McGwin, G., Griffin, R.L., 2014. The epidemiology of firework-related injuries in the United States: 2000–2010. Injury 45 (11), 1704–1709.

Moreno, T., Querol, X., Alastuey, A., Cruz Minguillón, M., Pey, J., Rodriguez, S., et al., 2007. Recreational atmospheric pollution episodes: inhalable metalliferous particles from firework displays. Atmos. Environ. 41 (5), 913–922.

Ng, N.L., Canagaratna, M.R., Zhang, Q., Jimenez, J.L., Tian, J., Ulbrich, I.M., et al., 2010. Organic aerosol components observed in Northern Hemispheric datasets from aerosol mass spectrometry. Atmos. Chem. Phys. 10 (10), 4625–4641.

Ng, N.L., Canagaratna, M.R., Jimenez, J.L., Chhabra, P.S., Seinfeld, J.H., Worsnop, D.R., 2011. Changes in organic aerosol composition with aging inferred from aerosol mass spectra. Atmos. Chem. Phys. 11 (13), 6465–6474.

Onasch, T.B., Trimborn, A., Fortner, E.C., Jayne, J.T., Kok, G.L., Williams, L.R., et al., 2012. Soot particle aerosol mass spectrometer: development, validation, and initial application. Aerosol. Sci. Technol. 46 (7), 804–817.

Perry, K.D., 1999. Effects of outdoor pyrotechnic displays on the regional air quality of Western Washington state. J. Air Waste Manage. Assoc. 49 (2), 146–155.

Pope, C.A.I., 2006. Health effects of fine particulate air pollution: lines that connect. Air Waste Manage Assoc. 56 (6), 709–742.

Pöschl, U., 2005. Atmospheric aerosols: composition, transformation, climate and health effects. Angew. Chem. Int. Ed. 44 (46), 7520–7540.

Retama, A., Neria-Hernández, A., Jaimes-Palomera, M., Rivera-Hernández, O., Sánchez-Rodríguez, M., López-Medina, A., et al., 2019. Fireworks: a major source of inorganic and organic aerosols during Christmas and New Year in Mexico City. Atmos. Environ. X 2.

Rissler, J., Nordin, E.Z., Eriksson, A.C., Nilsson, P.T., Frosch, M., Sporre, M.K., et al., 2014. Effective density and mixing state of aerosol particles in a near-traffic urban environment. Environ. Sci. Technol. 48 (11), 6300–6308.

Sasso, F., Picca, F., Pignatelli, A., Commodo, M., Minutolo, P., D'Anna, A., 2024. A laboratory study of secondary organic aerosol formation in an oxidation flow reactor. Fuel 367.

Seinfeld, J.H., Pandis, S.N., 2016. Atmospheric Chemistry and Physics: from Air Pollution to Climate Change, third ed. Wiley.

Steinhauser, G., Sterba, J.H., Foster, M., Grass, F., Bichler, M., 2008. Heavy metals from pyrotechnics in New Years Eve snow. Atmos. Environ. 42 (37), 8616–8622.

Toxicity of Military Smokes and Obscurants, 1999. National Academies Press, Washington, D.C.

Van Krevelen, D.W., 1950. Graphical-Statistical method for the study of structure and reaction processes of coal. Fuel 29, 228–269.

Vecchi, R., Bernardoni, V., Cricchio, D., D'Alessandro, A., Fermo, P., Lucarelli, F., et al., 2008. The impact of fireworks on airborne particles. Atmos. Environ. 42 (6), 1121–1132.

Wang, Y., Zhuang, G., Xu, C., An, Z., 2007a. The air pollution caused by the burning of fireworks during the lantern festival in Beijing. Atmos. Environ. 41 (2), 417–431.

Wang, Y., Zhuang, G., Xu, C., An, Z., 2007b. The air pollution caused by the burning of fireworks during the lantern festival in Beijing. Atmos. Environ. 41 (2), 417–431.

Webster, H.A., 1985. Visible spectra of standard navy colored flares. Propellants, Explos. Pyrotech. 10 (1), 1–4.

Xu, W., Croteau, P., Williams, L., Canagaratna, M., Onasch, T., Cross, E., et al., 2017. Laboratory characterization of an aerosol chemical speciation monitor with PM2.5 measurement capability. Aerosol. Sci. Technol. 51 (1), 69–83.

Zhang, Q., Rami Alfarra, M., Worsnop, D.R., Allan, J.D., Coe, H., Canagaratna, M.R., et al., 2005. Deconvolution and quantification of hydrocarbon-like and oxygenated organic aerosols based on aerosol mass spectrometry. Environ. Sci. Technol. 39 (13), 4938–4952.

Zhang, Q., Jimenez, J.L., Canagaratna, M.R., Allan, J.D., Coe, H., Ulbrich, I., et al., 2007. Ubiquity and dominance of oxygenated species in organic aerosols in anthropogenically-influenced northern hemisphere midlatitudes. Geophys. Res. Lett. 34 (13).

Zhang, Q., JJL, C.M.R., UIM, N.N.L., WDR, S.Y., 2011. Understanding atmospheric organic aerosols via factor analysis of aerosol mass spectrometry: a review. Anal. Bioanal. Chem. 401 (10), 3045–3067.
Zhang, J., Lance, S., Freedman, J.M., Sun, Y., Crandall, B.A., Wei, X., et al., 2019. Detailed measurements of submicron particles from an Independence day fireworks event in Albany, New York using HR-ToF-AMS. ACS Earth Space Chem. 3 (8), 1451–1459.
Zhu, W, Guo, S, Zhang, Z, Wang, H, Yu, Y, Chen, Z, et al., 2021. Mass Spectral Characterization of Secondary Organic Aerosol from Urban Cooking and Vehicular Sources. Atmos. Chem. Phys. 21, 15065–15079.